Design of a coated thinly clad chalcogenide long-period fiber grating refractive index sensor based on dual-peak resonance near the phase matching turning point

Qianyu Qi(齐倩玉)[1,2], Yaowei Li(李耀威)[1,2], Ting Liu(刘婷)[1,2], Peiqing Zhang(张培晴)[1,2,3,†], Shixun Dai(戴世勋)[1,2,3], and Tiefeng Xu(徐铁峰)[1,4]

[1] *Laboratory of Infrared Material and Devices, Advanced Technology Research Institute, Ningbo University, Ningbo* 315211, *China*
[2] *Key Laboratory of Photoelectric Detection Materials and Devices of Zhejiang Province, Ningbo* 315211, *China*
[3] *Engineering Research Center for Advanced Infrared Photoelectric Materials and Devices of Zhejiang Province, Ningbo University, Ningbo* 315211, *China*
[4] *Ningbo Institute of Oceanography, Ningbo* 315832, *China*

(Received 13 January 2022; revised manuscript received 13 March 2022; accepted manuscript online 1 April 2022)

A novel method for designing chalcogenide long-period fiber grating (LPFG) sensors based on the dual-peak resonance effect of the LPFG near the phase matching turning point (PMTP) is presented. Refractive index sensing in a high-refractive-index chalcogenide fiber is achieved with a coated thinly clad film. The dual-peak resonant characteristics near the PMTP and the refractive index sensing properties of the LPFG are analyzed first by the phase-matching condition of the LPFG. The effects of film parameters and cladding radius on the sensitivity of refractive index sensing are further discussed. The sensor is optimized by selecting the appropriate film parameters and cladding radius. Simulation results show that the ambient refractive index sensitivity of a dual-peak coated thinly clad chalcogenide LPFG at the PMTP can be 2400 nm/RIU, which is significantly higher than that of non-optimized gratings. It has great application potential in the field of chemical sensing and biosensors.

Keywords: chalcogenide longperiod fiber grating, dual-peak resonance, phase matching turning point, refractive index sensor

PACS: 42.68.Ay, 42.81.–i, 42.25.Dd, 42.81.Pa **DOI:** 10.1088/1674-1056/ac6338

1. Introduction

Long-period fiber gratings (LPFGs) promote optical coupling between the core mode and the cladding mode, and the peak value is easily affected by small changes in the surrounding refractive index (SRI). Thus, the refractive index sensing characteristics of a LPFG have attracted extensive attention and LPFGs have been widely used for biological and chemical sensing.[1–5] The phase matching curve (PMC) of each cladding mode of a LPFG contains a phase matching turning point (PMTP), and a LPFG working at the PMTP has the highest sensitivity to environmental disturbance.[6,7] When the actual grating period is less than the corresponding period of the PMTP, the LPFG has two resonance peaks that exhibit a dual-peak resonance effect.[8–10] At the same time, if the temperature,[11] ambient refractive index[12] and strain[13] change slightly, the bimodal resonant wavelength will change accordingly. Chen and Gu observed that a LPFG sensor based on bimodal resonance worked near the PMTP and had a high sensitivity to the SRI.[14] Shu *et al.* first studied the dual-peak resonance phenomenon of a LPFG and experimentally studied the response of the bimodal resonance to the SRI.[15] When the SRI increases, the two resonance summits move in the opposite direction.

Generally, the resonant wavelength of a LPFG has high sensitivity only when the SRI is slightly lower than the cladding refractive index.[16] However, the refractive index of traditional silica fiber is relatively small, and hence such fiber sensors will not work when special high-refractive-index liquids are encountered.[17] Furthermore, due to their limited transmission range, silica fiber sensors are powerless in the mid-infrared (MIR) range, which contains many important molecular spectral fingerprints.[18] Chalcogenide glasses (ChGs) are novel infrared (IR) optical materials with excellent infrared optical properties, such as a wide IR transmission range,[19] high linear and nonlinear refractive indices[20–22] and low phonon energy,[23] and ChG fibers are thus widely used in fiber lasers and biological and chemical sensors in the MIR range.[24–27]

However, due to the high refractive index of chalcogenide glass fiber (usually exceeding 2.0), its sensitivity is limited for conventional liquid detection. This problem can be solved by coating the fiber cladding with another thin film. Studies have found that coating a LPFG with a film having a refractive index higher than that of the cladding can expand the refractive index sensing range of the LPFG and improve its sensitivity.[28–32] Wang *et al.* proved that depositing a thin film at the PMTP of a LPFG can improve the sensitivity; they obtained a sensitivity of 9100 nm/RIU.[33] Nevertheless, when a high-refractive-index film is deposited on the optical fiber, the

†Corresponding author. E-mail: zhangpeiqing@nbu.edu.cn
© 2023 Chinese Physical Society and IOP Publishing Ltd

PMC will be changed, thereby leading to drifting of the PMTP. By reducing the fiber cladding radius, the PMC can also be changed.[34] Del Villar *et al.* proposed that reducing the fiber cladding radius and coating had opposite effects on the bimodal displacement.[35] Therefore, a LPFG can be controlled by reducing the cladding radius and coating until it works near the PMTP. Chen and Gu[36] studied the sensing characteristics of a thinly clad coated LPFG. Their results show that reduction of the cladding radius will increase the dynamic range of the high-sensitivity response of the LPFG thin film sensor.

In this paper, we design a chalcogenide LPFG with thin film coating, and study the refractive index sensing characteristics of a chalcogenide LPFG with a high-order mode PMTP. To optimize the performance, the influence of film parameters and cladding radius on the dual-peak resonance wavelength spacing is analyzed. By combining the two methods of plating high-refractive-index film outside the fiber and reducing the fiber radius, sensitivity of the chalcogenide LPFG for refractive index sensing is improved, thereby providing practical support and reference data for the design of a high-sensitivity chalcogenide LPFG refractive index sensor structure. It is expected that such a sensor could applied to the detection of various gases and liquids in the field of biological and chemical sensing.

2. Theoretical analysis

2.1. Simulation model

Figure 1(a) shows the transmission curve of fabricated As_2S_3 glass. The figure shows that this ChG has an extremely wide IR transmission area, which can be transparent from 1.0 μm to 14 μm; thus, the prepared ChG can be applied in the MIR spectral region. A graph of wavelength versus refractive index was produced using an infrared-variable angle spectroscopic ellipsometer (Mark II, J. A. Woollam, USA) and is shown in Fig. 1(b). This figure shows that the refractive index of As_2S_3 glass was greater than 2.3 in the IR region.

Figure 2 shows the structure and refractive index distribution of the coated thinly clad chalcogenide LPFG. The core and cladding are made of As_2S_3 glass, and the difference in refractive index between the core and the cladding is realized by fine-tuning the composition. A film material with a higher refractive index, such as diamond, graphite, graphene or carbon nanotubes, should be used for the coating. The refractive indices of the core and the cladding are n_1 and n_2, and their radii are a_1 and a_2, respectively. The refractive index of the film is n_3 and its thickness is $h = a_3 - a_2$. The refractive index of the external environment is n_{sur}. The optical fiber parameters used in the calculation are $a_1 = 3$ μm, $a_2 = 100$ μm, $n_1 = 2.4211$, $n_2 = 2.3952$, grating length $L = 4.5$ cm and the average refractive index change of the core is 1×10^{-2}.

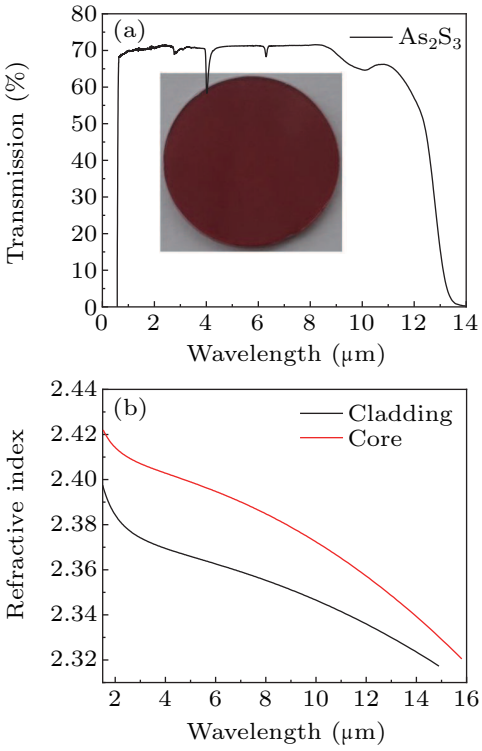


Fig. 1. (a) IR transmission spectra. (b) Graph of wavelength versus refractive index.

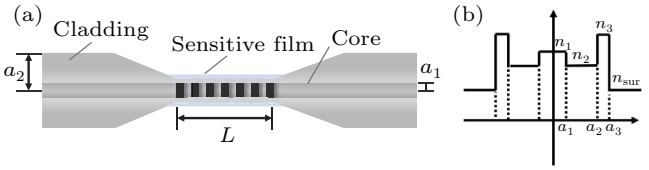


Fig. 2. Schematic of coated thinly clad chalcogenide LPFG: (a) structural model, (b) refractive index profile.

2.2. PMTP and dual-peak resonance

The phase matching condition of the LPFG, that is, the relationship between the grating period and resonant wavelength, is expressed as follows:

$$\lambda = \Delta n_{\text{eff}} \Lambda, \tag{1}$$

where $\Delta n_{\text{eff}} = n_{\text{eff}}^{\text{co}} - n_{\text{eff}}^{\text{cl}}$ is the effective refractive index difference between the core and the cladding, λ is the resonance wavelength and Λ is the grating period. According to the phase matching conditions, PMCs for low- and high-order cladding modes can be obtained, as shown in Figs. 3(a) and 3(b), respectively. When the grating period is short, the resonant wavelength of the low-order cladding mode increases monotonously with the grating period, whereas the PMC for the high-order cladding mode will exhibit a conic characteristic, and two wavelength values can satisfy Eq. (1). In other words, two resonance peaks appear in the transmission spectrum; this is called the double-peak effect. The higher the cladding mode sequence number, the smaller the grating period required for resonant coupling with the core mode, and

the smaller the resonant wavelength corresponding to the dual peak.

Cladding mode $LP_{0,19}$ with the cladding mode number $\nu = 19$ was first selected, and the characteristics of its PMTP were carefully studied. Figure 4 shows the PMC of the cladding mode $LP_{0,19}$. One PMTP is found in the PMC; the corresponding period is 110.5 μm and the slope is infinite at the PMTP. When the period is less than 110.5 μm double-peak resonance occurs (as shown in the inset in Fig. 4). When the LPFG is affected by the refractive index it will cause a change in the refractive index of the cladding mode; this will then cause a change in the resonant wavelength. When the grating period approaches the PMTP, a LPFG refractive index sensor with high sensitivity will be obtained.

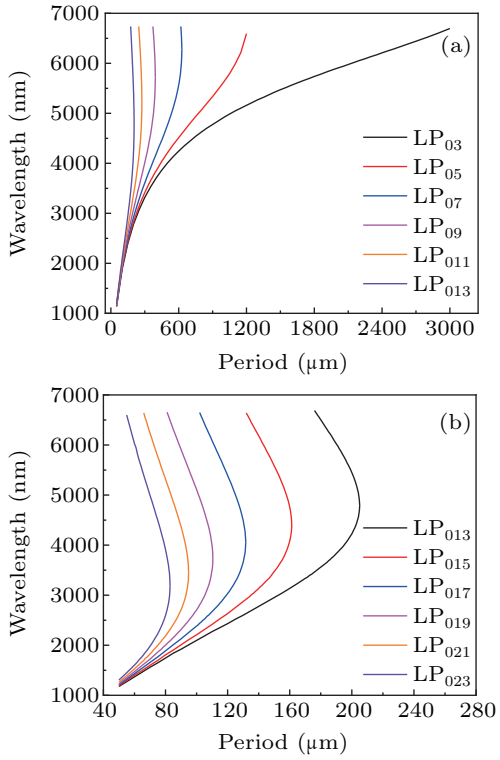


Fig. 3. Phase-matching curves of odd cladding modes for (a) low-order cladding and (b) high-order cladding.

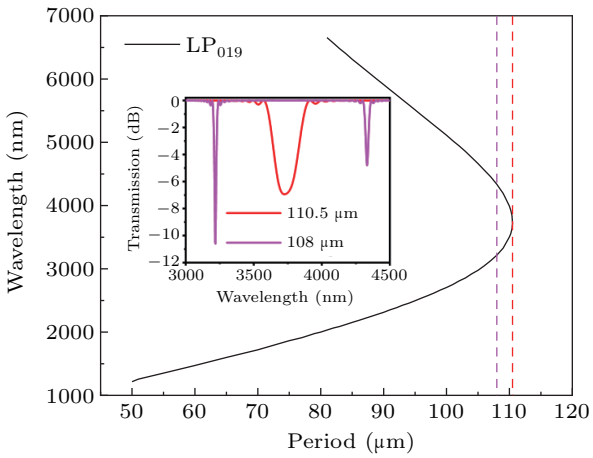


Fig. 4. Phase-matching curve of $LP_{0,19}$.

3. Characteristics of LPFG refractive index sensing operating at the PMTP

When the double peaks are located near the PMTP the slope of the PMC approaches infinity near the turning point; that is, the wavelength is most sensitive to periodic changes, thereby leading to a very high sensitivity to changes in the external environment. Figures 5(a), 6(a), and 7(a) show the

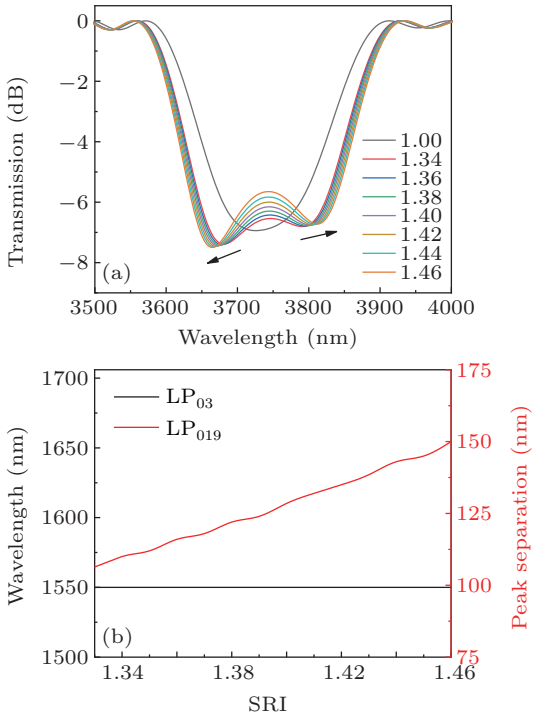


Fig. 5. (a) Transmission spectrum of the $LP_{0,19}$ mode and (b) response of $LP_{0,3}$ and $LP_{0,19}$ modes to the SRI for SRI = 1.34–1.46.

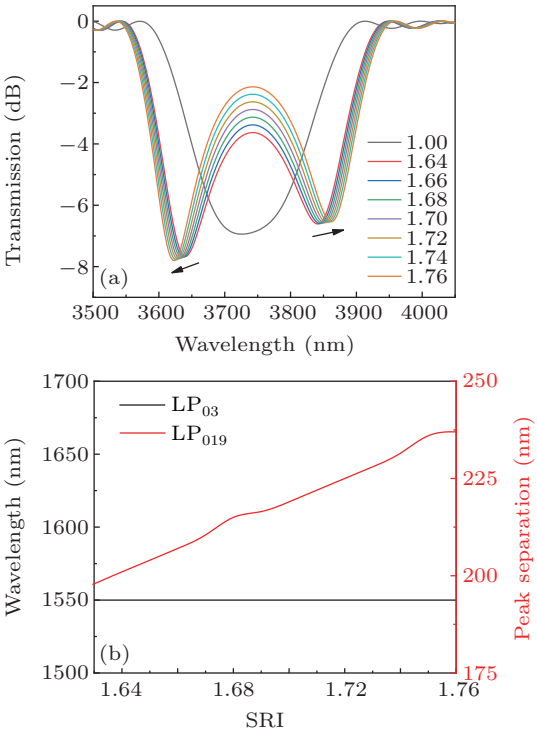


Fig. 6. (a) Transmission spectrum of the $LP_{0,19}$ mode and (b) the response of $LP_{0,3}$ and $LP_{0,19}$ modes to the SRI for SRI = 1.64–1.76.

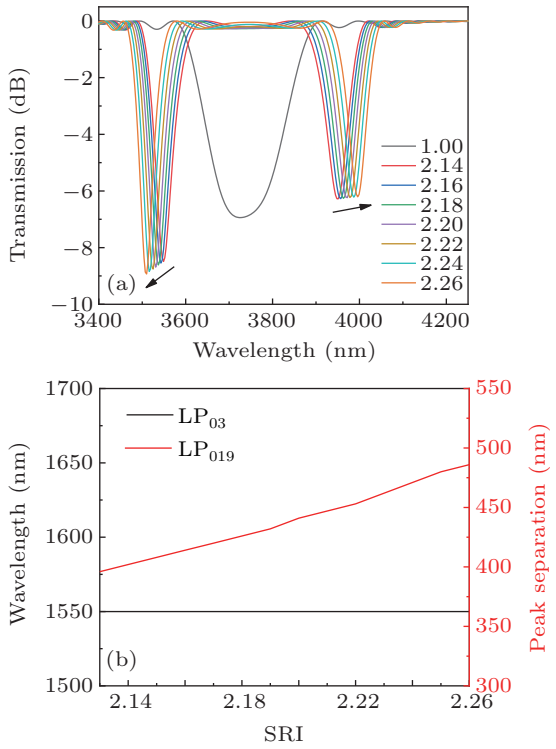


Fig. 7. (a) Transmission spectrum of the $LP_{0,19}$ mode and (b) the response of $LP_{0,3}$ and $LP_{0,19}$ modes to the SRI for SRI = 2.14–2.26.

transmission spectra of $LP_{0,19}$ cladding modes at a low (1.34–1.46), medium (1.64–1.76), and high (2.14–2.26) SRI when the grating period is 110.5 μm. Figures 5(b), 6(b), and 7(b) show the responses of low-order ($LP_{0,3}$ modes) and high-order cladding modes ($LP_{0,19}$ modes) to different SRIs. When the period is 110.5 μm the low-order cladding mode is unimodal and almost unresponsive to all refractive index environments, whereas the high-order cladding modes have different responses to various SRIs. As the refractive index increases, the peak separation rises continuously. High-sensitivity detection of the SRI is realized by detecting the bimodal wavelength spacing. Thus, compared with low-order cladding modes, selecting a high-order cladding mode in the structural design can produce higher sensitivity refractive index sensing.

4. Structure optimization

4.1. Film parameters

A LPFG is highly sensitive to the environment because the electromagnetic field of the cladding mode penetrates into the environment in the form of an evanescent wave at the interface between the cladding and the environment and interacts with the external environment, thereby changing the effective refractive index of the cladding mode and leading to drifting of the resonant wavelength.[37] After coating the LPFG with a film whose refractive index is much higher than that of the cladding material, the core mode is unaffected by the film, and the parameters of the film mainly affect the effective refractive index of the cladding mode, thus affecting the resonant wavelength of the grating.

The refractive index of the film in the calculation is selected as $n_3 = 2.45$. First, the external environment is assumed to be air ($n_4 = 1$). When the film thickness increases from 0 nm to 1000 nm, numerical simulations obtain the relationship between the effective refractive index and the film thickness of $LP_{0,3}$–$LP_{0,23}$ odd-numbered cladding modes (Fig. 8(a)). The effective refractive index of each cladding mode gradually increases with the thickness of the film.

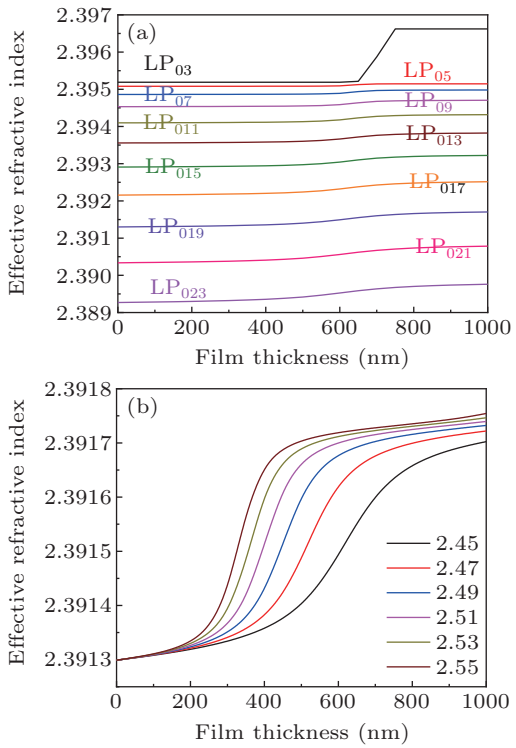


Fig. 8. Variation of effective refractive index of (a) odd-numbered cladding modes with film thickness and (b) the $LP_{0,19}$ cladding mode with film parameters.

The external environment is set to be air and the $LP_{0,19}$ cladding mode is selected, as shown in Fig. 8(b). When the film thickness is fixed, changing the refractive index of the film can also alter the effective refractive index of the cladding mode. In addition, the effective refractive index of the cladding mode will show abrupt changes within a specific film thickness range, and the range of abrupt changes of films with different refractive indices will vary. For example, when the film refractive index is 2.45, the effective refractive index in the corresponding cladding mode changes from 300 nm to 700 nm, and when the film refractive index is 2.55, the corresponding change in the effective refractive index of the cladding mode is from 200 nm to 600 nm. When the film increases to a certain thickness, the low-order cladding mode will enter the film layer for transmission, and the original high-order mode will replace the low-order mode step by step. At this time, the energy of the electromagnetic field is redistributed among the cladding modes, the lowest cladding

mode is transferred to the thin film layer for transmission and the higher-order mode covers the energy state of its previous mode, thus affecting the effective refractive index. Villar *et al.* explained this from the viewpoint of mode conversion.[38] When mode conversion of a cladding mode occurs, the effective refractive index of each cladding mode changes sharply. A sudden change in the effective refractive index of the cladding mode will inevitably lead to a shift in the resonance wavelength, indicating that a suitable refractive index and thickness of the film layer must be determined so that the coated LPFG works in the region of the effective refractive index of the cladding mode. A small change will cause a large change in the cladding mode, which will cause a significant change in the resonance wavelength and improve the sensitivity of LPFG refractive index sensing.

4.2. Cladding radius

The design in this work adopts a film refractive index $n_3 = 2.55$ and film thickness $h = 300$ nm because the choice of a high-refractive-index material can help shorten the coating time and save costs. The refractive index of carbon-based materials (carbon, diamond, graphite, graphene, carbon nanotubes) is $n = 2.4$ to $n = 2.9$, which is much higher than that of the cladding material. Amorphous carbon film materials such as graphene/carbon nanotube composite material has excellent properties (high hardness, wear resistance, low friction coefficient, optical transmittance, chemical inertness) and are suitable as coating materials. Many papers have reported the use of carbon-based materials such as graphene in the field of optical fiber sensing, and a variety of coating methods have been proposed.[39–41] Among these, a method suitable for application with chalcogenide optical fibers is the combined dispersion rotary coating method. The process of preparing graphene/carbon nanotube composites by the mixed dispersion rotary coating method is as follows. First, a graphene/carbon nanotube composite dispersion with uniform dispersion is prepared. The mixed dispersion is then sonicated and deposited on different substrates by a rotary coating method. The thickness of the composite film can be controlled according to the speed and time of spin coating.

Coating the optical fiber with a high-refractive-index film will change the PMC. Figure 9(a) shows the PMC of the $LP_{0,19}$ cladding mode when it is uncoated, and the film thickness is 300 nm. Obviously, deposition of the film causes the curve to move to a longer period. In other words, if the period is designed to be 110.5 μm, for which the uncoated LPFG works at the turning point, when a 300 nm thick film is deposited on the optical fiber, dual-peak resonance will occur. In addition, the thicker the film, the greater the separation between the two peaks will be. To solve this problem, we propose reducing the bimodal spacing of the coated grating by reducing the fiber radius. Figure 9(b) shows that the peak separation decreases with a decrease in the cladding radius. When the cladding radius is 99.53 μm, the peak separation is 0. By optimizing the fiber radius, the bimodal grating works near the PMTP and optimal sensitivity can be achieved.

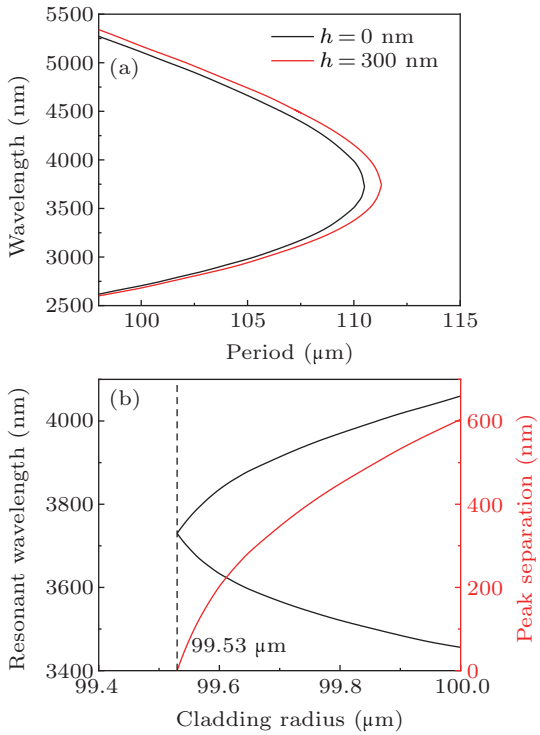


Fig. 9. (a) Effect of film thickness on phase matching curve. (b) Variation of peak separation with cladding radius.

5. LPFG refractive index sensing characteristics of coated thinly clad fiber operating at the PMTP

The refractive index sensing performance of the chalcogenide LPFG is optimized by a combination of high-order mode coupling characteristics of the LPFG and a reduction of the cladding radius and surface modification of the sensitive film. Figures 10(a), 11(a), and 12(a) show the transmission spectra of $LP_{0,19}$ cladding modes at low (1.34–1.46), medium (1.64–1.76), and high (2.14–2.26) SRIs when the film thickness $h = 300$ nm, the film refractive index $n_3 = 2.55$, the cladding radius $a_2 = 99.53$ μm and the period $\Lambda = 110.5$ μm. The bimodal spacing increases with the SRI.

Figures 10(b), 11(b), and 12(b) show the linear fitting relationship between peak separation and different SRIs before and after optimization. The sensitivity of peak separation to changes in the SRI can be defined as

$$S_{\mathrm{SRI}} = \frac{\Delta\lambda_{\mathrm{res}}}{\Delta n_{\mathrm{sur}}}. \tag{2}$$

That is, the shift of the dual-peak resonance wavelength produced by unit change in the SRI is used to characterize the speed of the change in the double-peak spacing with the

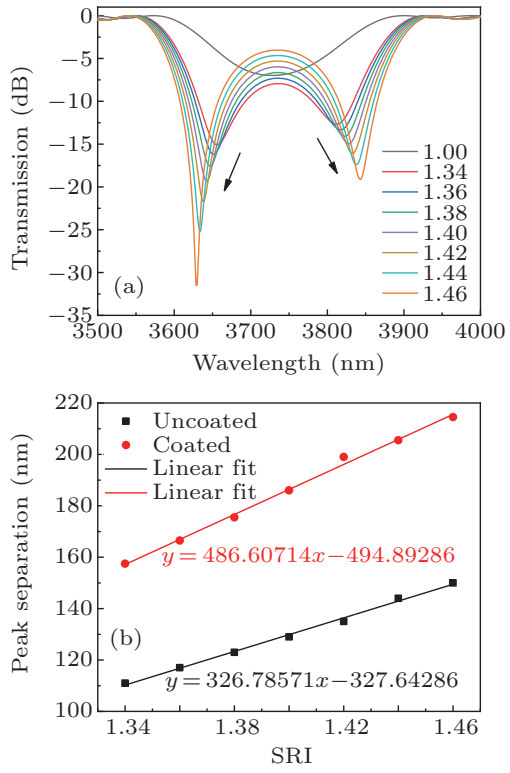


Fig. 10. (a) Transmission spectrum of the $LP_{0,19}$ mode and (b) sensitivities before and after optimization for SRI = 1.34–1.46.

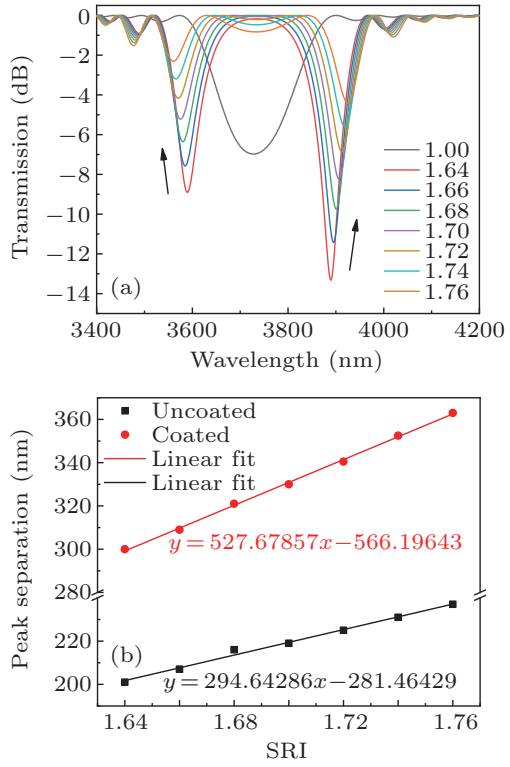


Fig. 11. (a) Transmission spectrum of the $LP_{0,19}$ mode and (b) sensitivities before and after optimization for SRI = 1.64–1.76.

SRI. When the SRI is between 1.34 and 1.46, the unoptimized bimodal LPFG refractive index sensing sensitivity is 326 nm/RIU, whereas the optimized bimodal LPFG refractive index sensitivity is 486 nm/RIU, the sensitivity being increased by 160 nm/RIU. When the SRI changes from 1.64 to 1.76, the sensitivity of the refractive index sensor before and after optimization is 294 nm/RIU and 527 nm/RIU, respectively, the sensitivity being increased by 233 nm/RIU. When the SRI increases from 2.14 to 2.26, the wavelength spacing of the bimodal LPFG rises from 711 nm to 1003 nm. The refractive index sensitivity of the optimized bimodal LPFG reaches 2400 nm/RIU, whereas the refractive index sensing sensitivity of the unoptimized bimodal LPFG is only 701 nm/RIU; the sensitivity is increased by 1699 nm/RIU. These results show that by selecting appropriate grating parameters, film parameters and cladding radius, the refractive index sensitivity of the sensor is greatly improved compared with that of a generalized LPFG refractive index sensor. The new LPFG refractive index sensor has high sensitivity and good linearity and is expected to be applied in the fields of gas, liquid, chemistry and biological sensing.

In order to compare the sensitivity of the sensor presented in this paper to the SRI with that of some other sensors, the average sensitivity to the SRI and detection range of several typical LPFG SRI sensors are listed in Table 1. The results show that although the sensitivity of most quartz fiber grating sensors is high, the range of refractive index in which they can work is relatively limited. Moreover, when the sensitivity of a quartz fiber grating sensor is too high, its stability will become poor. Considering the relationship between equilibrium stability and sensitivity, we chose the above structural parameters. Therefore, the structural design proposed by us not only widens the detection range but also has a certain stability.

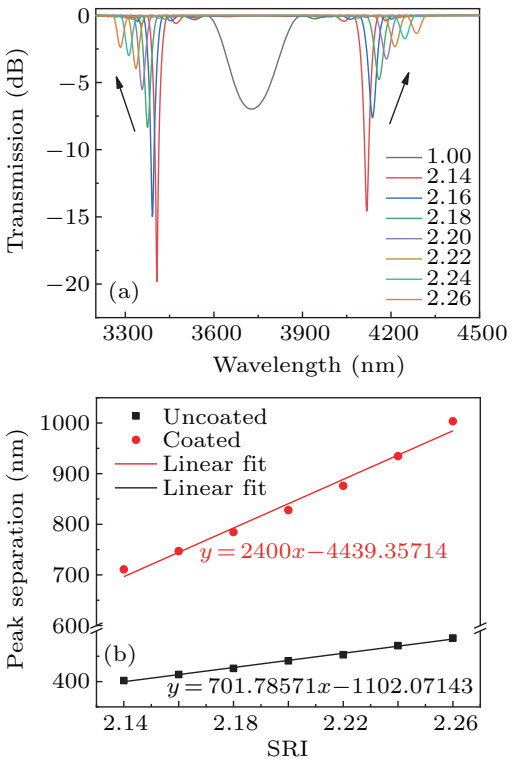


Fig. 12. (a) Transmission spectrum of the $LP_{0,19}$ mode and (b) sensitivities before and after optimization for SRI = 2.14–2.26.

Table 1. Sensitivity of different LPFG sensors.

Sensors	Materials	Average sensitivity (nm/RIU)	Detection range	Reference
LPFG sensor based on mode transition near the PMTP	SMF-28	4900	1.34–1.39	[34]
Modulated cascaded coated LPFG based on the PMTP	SMF-28	9670	1.3300–1.3345	[42]
Etched LPFG sensor near the PMTP	SMF-28	5602	1.37–1.41	[43]
Dual-peak LPFG sensor	SMF-28	2500	1.333–1.353	[44]
Coated LPFG sensor based on the PMTP	SMF-28	2138	1.335–1.373	[45]
π-phase-shifted LPFG sensor near the PMTP	SMF-28	9093.3	1.33–1.34	[46]
Few-mode LPFG sensor based on dual-peak resonance	SMF-28	1114.28	1.33–1.34	[47]
Etched dual-peak LPFG sensor	SMF-28	2670	1.300–1.440	[48]
Coated thinly clad LPFG sensor near PMTP	ChG	2400	1.34–2.26	this work

6. Conclusion

In this paper, a coated thinly clad chalcogenide LPFG refractive index sensor based on the PMTP dual-peak resonance effect is studied theoretically. The sensor is optimized by selecting appropriate film parameters and cladding radius, and the sensitivity of the chalcogenide LPFG refractive index sensor is greatly improved. The simulation results show that the sensitivity of the coated thinly clad chalcogenide LPFG at the PMTP to the SRI is 2400 nm/RIU, which is significantly higher than that of a non-optimized grating. The structure proposed in this work not only has a wider sensing range but also offers a more flexible sensing scheme. Suitable sensitive materials can be selected according to the environmental object to be detected. High sensitivity can be obtained by adjusting the parameters of the film or the grating structure and is expected to be obtained in widely used photochemical biosensors.

Acknowledgments

Project supported by the Natural Science Foundation of China (Grant Nos. 62075107, 61935006, 62090064, and 62090065) and K. C. Wong Magna Fund in Ningbo University.

References

[1] Gan W B, Xu Z L, Li Y W, Bi W C, Chu L Y, Qi Q Y, Yang Y T, Zhang P Q, Gan N, Dai S X and Xu T F 2022 *Biosens. Bioelectron.* **199** 113860
[2] Esposito F, Sansone L, Taddei C, Campopiano S, Giordano M and Iadicicco A 2018 *Sens. Actuators B Chem.* **274** 517
[3] Wang R D, Ren Z Y, Kong D P, Hu B W and He Z Q 2020 *Opt. Mater.* **109** 110253
[4] Yu S, Ding L Y, Lin H T, Wu W and Huang J 2019 *Biosens. Bioelectron.* **146** 111760
[5] Tiwari D, Mullaney K, Korposh S, James S W, Lee S W and Tatam R P 2017 *Sens. Actuators B Chem.* **242** 645
[6] Shu X W, Zhang L and Bennion I 2001 *Opt. Lett.* **26** 1755
[7] Shu X W, Zhang L and Bennion I 2002 *J. Light. Technol.* **20** 255
[8] Gu Z T, Ling Q, Lan J L and Gao K 2017 *Opt. Laser Technol.* **96** 249
[9] Gu Z T, Shi Y J and Zhang J T 2012 *Opt. Eng.* **51** 081508
[10] Gu Z T, Xu Y P, Deng C L and Zhang J T 2009 *J. Opt. A: Pure Appl. Opt.* **11** 085701
[11] Wong R Y, Chehura E, Staines S E, James S W and Tatam R P 2014 *Appl. Opt.* **53** 4669
[12] Zhou W, Ran Y L, Yan Z J, Sun Q Z, Liu C and Liu D M 2020 *Sensors* **20** 5978
[13] Guan T Q, Gu Z T, Ling Q and Feng W B 2019 *Opt. Laser Technol.* **114** 20
[14] Chen H Y and Gu Z T 2012 *Meas. Sci. Technol.* **23** 035105
[15] Shu X W and Huang D X 1999 *Opt. Commun.* **171** 65
[16] Patrick H J, Kersey A D and Bucholtz F 1998 *J. Light. Technol.* **16** 1606
[17] Iadicicco A, Campopiano S, Giordano M and Cusano A 2007 *Appl. Opt.* **46** 6945
[18] Su J X, Dai S X and Gan N 2020 *Opt. Express* **28** 184
[19] Shiryaev V S and Churbanov M F 2013 *J. Non. Cryst. Solids* **377** 225
[20] Shang H Y, Zhang M J, Sun D D, Liu Y G, Wang Z, Liu D and Zeng S Q 2021 *Results Phys.* **28** 104552
[21] Sahoo D, Priyadarshini P, Aparimita A, Alagarasan D, Ganesan R, Varadharajaperumal S and Naik R 2021 *Opt. Laser Technol.* **140** 107036
[22] Yang Z, Hu H N, Li Q L, Zhang Z, Niu L, Wu J, Wei T X, Sun Y H, Fang Y M, Wang X S, Yang Z Y, Zhou J F and Wang R P 2021 *Opt. Mater.* **117** 111208
[23] Gai X, Han T, Prasad A, Madden S, Choi D Y, Wang R P, Bulla D and Luther-Davies B 2010 *Opt. Express* **18** 26635
[24] Bureau B, Boussard C, Cui S, Chahal R, Anne M L, Nazabal V, Sire O, Loréal O, Lucas P, Monbet V, Doualan J L, Camy P, Tariel H, Charpentier F, Quetel L, Adam J L and Lucas J 2014 *Opt. Eng.* **53** 027101
[25] Sharma A K and Gupta J 2018 *Opt. Fiber Technol.* **41** 125
[26] Sharma A K and Kaur B 2018 *Opt. Fiber Technol.* **43** 163
[27] Bureau B, Maurugeon S, Charpentier F, Adam J L, Boussard-Plédel C and Zhang X H 2009 *Fiber Integr. Opt.* **28** 65
[28] Luo B B, Liu Z J, Wang X, Shi S H, Zhong N B, Ma P J, Wu S X, Wu D C, Zhao M F and Liang W W 2021 *J. Biophoton.* **14** e202000279
[29] Xu B, Huang J, Ding L Y, Zhang H and Zhang H W 2021 *IEEE Sens. J.* **21** 16691
[30] Tan S Y, Lee S C, Kuramitz H and Abd-Rahman F 2019 *Optik* **194** 163040
[31] Yan H H, Wang L, Li S F, Wang J, Zhang H S, Cheng P and Pan Y 2019 *Opt. Eng.* **58** 066109
[32] Khaliq S, W. James S and P. Tatam R 2001 *Opt. Lett.* **26** 1224
[33] Del Villar I, Cruz J L, Socorro A B, Corres J M and Matias I R 2016 *Opt. Express* **24** 17680
[34] Ling Q, Gu Z T, Jiang X L and Gao K 2019 *Opt. Commun.* **439** 187
[35] Wang Z Y, Heflin J R. Stolen R H and Ramachandran S 2005 *Opt. Express* **13** 2808
[36] Chen H Y and Gu Z T 2013 *Optik* **124** 219
[37] Quero G, Crescitelli A, Paladino D, Consales M, Buosciolo A, Giordano M, Cutolo A and Cusano A 2011 *Sens. Actuators B Chem.* **152** 196
[38] Del I, Achaerandio M, Matias, I R and Arregui F J 2005 *Opt. Lett.* **30** 720
[39] Luo B, Liu Z, Wang X, Shi S, Zhong N, Ma P, Wu S, Wu D, Zhao M and Liang W 2021 *J. Biophoton.* **14** e202000279
[40] Wang R D, Ren Z Y, Kong X D, Kong D P, Hu B W and He Z Q 2020 *J. Phys. D: Appl. Phys.* **53** 065104
[41] Sangeetha M and Madhan D 2020 *Opt. Laser Technol.* **127** 106193
[42] Feng W B, Gu Z T, Ling Q and Sang J G 2017 *J. Opt.* **19** 125703
[43] Ling Q, Gu Z T and Gao K 2018 *Appl. Opt.* **57** 2693
[44] Garg R, Tripathi S M, Thyagarajan K and Bock W J 2013 *Sens. Actuators B Chem.* **176** 1121
[45] Zhou W, Ran Y L, Yan Z J, Sun Q Z, Liu C and Liu D M 2020 *Sensors* **20** 5978
[46] Jiang H P, Gu Z T, Zhou Y, Wu J Y, Li Z Y and Yan Y X 2022 *Optik* **251** 168349
[47] Ling Q and Gu Z T 2019 *J. Opt. Soc. Am. B* **36** 2210
[48] Chen X F, Zhou K M, Zhang L and Bennion I 2007 *Appl. Opt.* **46** 451